Bioorganic Chemistry 92 (2019) 103237

Contents lists available at ScienceDirect

Bioorganic Chemistry

journal homepage: www.elsevier.com/locate/bioorg

NO inhibitory diterpenoids as potential anti-inflammatory agents from *Euphorbia antiquorum*

Lijun An[a,1], Yue Liang[a,1], Xueyuan Yang[a], Huimei Wang[a], Jie Zhang[b], Muhetaer Tuerhong[c], Dihua Li[d], Chunyan Wang[e], Dongho Lee[f], Jing Xu[a,*], Ling Shuai[a], Jin Jin[a], Yuanqiang Guo[a,g,*]

[a] State Key Laboratory of Medicinal Chemical Biology, College of Pharmacy, Tianjin Key Laboratory of Molecular Drug Research, and Drug Discovery Center for Infectious Disease, Nankai University, Tianjin 300350, People's Republic of China
[b] Key Laboratory for Green Processing of Chemical Engineering of Xinjiang Bingtuan, School of Chemistry and Chemical Engineering, Shihezi University, Shihezi 832003, People's Republic of China
[c] College of Chemistry and Environmental Sciences, Laboratory of Xinjiang Native Medicinal and Edible Plant Resources Chemistry, Kashgar University, Kashgar 844000, People's Republic of China
[d] Tianjin Institute of Acute Abdominal Diseases of Integrated Traditional Chinese and Western Medicine, Nankai Hospital Affiliated to Nankai University, Tianjin 300100, People's Republic of China
[e] Tianjin Second People's Hospital, Tianjin 300192, People's Republic of China
[f] Department of Biosystems and Biotechnology, College of Life Sciences and Biotechnology, Korea University, Seoul 136-713, Republic of Korea
[g] State Key Laboratory for Chemistry and Molecular Engineering of Medicinal Resources, Guangxi Normal University, Guilin 541004, People's Republic of China

ARTICLE INFO

Keywords:
NO inhibitory effects
Euphorbia antiquorum
Diterpenoids
Inflammation
Molecular docking

ABSTRACT

Two new *ent*-atisane-type diterpenoids (**1** and **2**), three new lathyrane-type diterpenoids (**3–5**), and seven known analogues (**6–12**) were isolated from *Euphorbia antiquorum*. The structures of these diterpenoids were established by analysis of their NMR, MS, and electronic circular dichroism data. The anti-inflammatory activities were evaluated biologically and compounds **1**, **4**, **7**, **8**, and **10** displayed strong NO inhibitory effects with IC_{50} values less than 40 μM. The potential anti-inflammatory mechanism was also investigated using molecular docking and Western blotting.

1. Introduction

It has evidenced that inflammation, especially chronic inflammation, is involved in the pathogenesis of a variety of diseases, such as atherosclerosis [1], obesity, metabolic syndrome [2], diabetes [3], neurodegenerative diseases [4], and even several types of cancers [5]. Thus, to inhibit inflammation is considered to be beneficial and helpful for the prevention of the above mentioned diseases. When inflammation happens, the crucial proteins iNOS and COX-2 in the inflammatory signaling pathway usually have a high-expression and catalyze to produce massive inflammation mediators, such as NO and PGE_2 [6]. Considering that excessive inflammation mediators are an obvious sign indicating inflammatory response, to inhibit the generation of these inflammatory factors has thus become an applicable strategy to resist inflammation. In addition to synthetic compounds available for the inhibition of inflammatory factors, bioactive natural products are also considered as an indispensable choice due to the structural and biological diversity and the potential value as drug lead compounds in drug discovery.

The genus *Euphorbia* Linn., belonging to the Euphorbiaceae plant family, contains about 2000 species widely distributed in tropical and temperate regions. There are about 80 species growing in China. Some *Euphorbia* species have been used historically as folk medicines for multiple medical indications in China and other countries [7,8]. Chemical investigations on this genus have led to the isolation of a large array of diterpenoids with structural diversity, such as jatrophane, lathyrane, tigliane, ingenane, myrsinol, and ingol types, which exhibited various biological activities including cytotoxic, anti-leukemic insecticidal, antimicrobial, and anti-inflammatory effects [9–33]. The species *Euphorbia antiquorum* L. is a small tree distributed mainly in the tropical region of Asia. This plant has been used as a folk medicine in mainland China for the treatment of dropsy, abdominal lump, diarrhea, scabies, and dyspepsia [34]. In our ongoing search for bioactive natural products as NO inhibitors for inflammatory diseases from plants

* Corresponding authors at: State Key Laboratory of Medicinal Chemical Biology, College of Pharmacy, Tianjin Key Laboratory of Molecular Drug Research, and Drug Discovery Center for Infectious Disease, Nankai University, Tianjin 300350, People's Republic of China.
E-mail addresses: xujing611@nankai.edu.cn (J. Xu), victgyq@nankai.edu.cn (Y. Guo).
[1] These authors contributed equally to this work.

https://doi.org/10.1016/j.bioorg.2019.103237
Received 12 June 2019; Received in revised form 26 August 2019; Accepted 30 August 2019
Available online 04 September 2019
0045-2068/

[35–37], *Euphorbia* plants rich in various types of terpenoids evoked our great interest and the subordinate species *E. antiquorum* was investigated. This procedure led to the isolation of five new diterpenoids, designated as euphorins A − E (**1–5**), along with seven known diterpenoids (**6–12**) from the methanol extract of the stems of *E. antiquorum*. The structures of these diterpenoids were established by NMR, MS, and electronic circular dichroism (ECD) data analysis. All of the isolates showed inhibitory activities toward lipopolysaccharide (LPS)-induced NO production in murine microglial BV-2 cells. Herein, we describe the structural determination and anti-inflammatory activities of these isolated diterpenoids as well as the possible anti-inflammatory mechanism.

2. Experimental

2.1. General experimental procedures

Optical rotations were recorded on an InsMark IP120 automatic polarimeter (InsMark Instrument Co., Ltd., Shanghai, People's Republic of China). ECD spectra were obtained on a JASCO J-715CD spectrometer (JASCO Corporation, Tokyo, Japan). Infrared (IR) spectra (KBr disks) were recorded on a Bruker Tensor 27 FT-IR spectrometer. 1D and 2D NMR experiments were performed on a Bruker AV 400 instrument (Bruker, Switzerland, 100 MHz for ^{13}C and 400 MHz for ^{1}H) with TMS as an internal reference at room temperature. ESIMS and HRESIMS data were acquired on a Thermo Finnigan LCQ-Advantage mass spectrometer and an IonSpec 7.0 T FTICR MS (IonSpec Co., Ltd., Lake Forest, CA), respectively. HPLC separations were conducted on a CXTH system, equipped with a Shodex RI-102 detector (Showa Denko Co., Ltd., Tokyo, Japan) and a YMC-pack ODS-AM (20 × 250 mm) column (YMC Co. Ltd., Kyoto, Japan). Medium pressure liquid chromatography (MPLC) was run on a P0100 pump with an ultraviolet (UV) detector (Huideyi Co., Beijing, People's Republic of China) and a column (40 × 400 mm) filled by octadecylsilyl (ODS, 50 μm, YMC Co., Ltd.). Silica gel (200–300 mesh) used for column chromatography was purchased from Qingdao Haiyang Chemical Group Co., Ltd. (Qingdao, People's Republic of China). Chemical reagents (analytical grade) and biological reagents were provided by Tianjin Chemical Reagent Co. (Tianjin, People's Republic of China) and Sigma Co., respectively. The BV-2 cell line was from Shanghai Institutes for Biological Sciences, Chinese Academy of Sciences (Shanghai, People's Republic of China).

2.2. Plant material

The stems of *E. antiquorum* were collected from Guangxi Zhuang Autonomous Region, People's Republic of China, in November 2016. The botanical identification was made by one of the authors (Y. Guo), and a voucher specimen (No. 20161101A) representing this collection has been deposited in College of Pharmacy, Nankai University, Tianjin, People's Republic of China.

2.3. Extraction and isolation

The stems of *E. antiquorum* (11.5 kg) were cut into pieces. After drying, the stems were extracted with MeOH (3 × 60 L) under reflux. The organic solvent was evaporated to give a crude methanol extract (400 g), which was suspended in H_2O (0.4 L) and then partitioned with petroleum ether (5 × 0.4 L) to give the petroleum ether-soluble portion (258 g). This portion was fractionated by silica gel column chromatography (silica gel, 1350 g; column, 9 × 70 cm), using a gradient solvent system of petroleum ether-acetone (100: 0, 100: 2, 100: 4, 100: 6, 100: 8, 100: 11, 100: 16, 100: 23, 100: 30, 21 L for each gradient elution), to afford nine fractions (F_1 − F_9) according to the TLC analysis. Fraction F_7 was further separated by MPLC over octadecylsilane (ODS) eluting with a step gradient of 64–92% MeOH in H_2O to give eight subfractions $F_{7\text{-}1}$ − $F_{7\text{-}8}$. The subsequent purification of $F_{7\text{-}2}$ (68% MeOH in H_2O) by preparative HPLC (YMC-pack ODS-AM column, 20 × 250 mm) afforded compound **1** (t_R = 38 min, 6.5 mg). Using the above MPLC, fraction F_3 (72–92% MeOH in H_2O) yielded eight subfractions $F_{3\text{-}1}$–$F_{3\text{-}8}$. With the same HPLC system, compound **2** (t_R = 32 min, 6.9 mg) was isolated from $F_{3\text{-}2}$ (79% MeOH in H_2O). Using the same procedure as for fraction F_3, fraction F_8 gave five subfractions $F_{8\text{-}1}$–$F_{8\text{-}5}$, and the purification of subfractions $F_{8\text{-}2}$ (70% MeOH in H_2O) and $F_{8\text{-}4}$ (78% MeOH in H_2O) resulted in the isolation of compounds **3** (t_R = 29 min, 8.4 mg) and **11** (t_R = 41 min, 26.9 mg), respectively, with the above HPLC. Fraction F_5 was fractionated by the above MPLC to afford subfractions $F_{5\text{-}1}$–$F_{5\text{-}9}$. The following purification was performed using the above HPLC. Compounds **4** (t_R = 30 min, 5.7 mg) and **7** (t_R = 29 min, 50.8 mg) were isolated from $F_{5\text{-}4}$ (81% MeOH in H_2O), compounds **5** (t_R = 43 min, 9.9 mg) and **6** (t_R = 36 min, 9.9 mg) were obtained from $F_{5\text{-}3}$ (75.5% MeOH in H_2O), and the purification of subfraction $F_{5\text{-}5}$ (80% MeOH in H_2O) gave compound **8** (t_R = 57 min, 11.9 mg). Using the same MPLC as applied for the above fractions, subfractions $F_{2\text{-}1}$–$F_{2\text{-}8}$, $F_{4\text{-}1}$–$F_{4\text{-}7}$, and $F_{6\text{-}1}$–$F_{6\text{-}5}$ were obtained from fractions F_2, F_4, and F_6, respectively. The susequent purification of subfractions $F_{2\text{-}2}$ (85% MeOH in H_2O), $F_{4\text{-}3}$ (81% MeOH in H_2O), and $F_{6\text{-}5}$ (89.5% MeOH in H_2O) with the same HPLC led to the acquirement of compounds **9** (t_R = 24 min, 5.5 mg), **10** (t_R = 33 min, 12.9 mg), and **12** (t_R = 53 min, 35.6 mg), respectively.

2.3.1. Euphorin A (1)

Colorless oil; [α] + 31.2 (*c* 0.2, CH_2Cl_2); ECD (CH_3CN) 218 (Δε –0.88), 313 (Δε + 0.79) nm; IR (KBr) ν_{max} cm^{-1}: 3436, 2869, 2857, 1707, 1438, 1387, 1186, 733; ^{13}C NMR (100 MHz, $CDCl_3$) data and ^{1}H NMR (400 MHz, $CDCl_3$), see Tables 1 and 2; ESIMS *m/z* 411 $[M+Na]^+$; HRESIMS *m/z* 411.2145 $[M+Na]^+$, calcd for $C_{23}H_{32}NaO_5$, 411.2147.

2.3.2. Euphorin B (2)

Amorphous powder; [α] − 3.3 (*c* 0.1, CH_2Cl_2); ECD (CH_3CN) 214 (Δε − 1.59), 297 (Δε + 0.78) nm; IR (KBr) ν_{max} cm^{-1}: 2926, 2857, 1711, 1459, 1387, 1182, 889; ^{13}C NMR (100 MHz, $CDCl_3$) data and ^{1}H NMR (400 MHz, $CDCl_3$), see Tables 1 and 2; ESIMS *m/z* 395 $[M + Na]^+$; HRESIMS *m/z* 395.2197 $[M + Na]^+$, calcd for $C_{23}H_{32}NaO_4$, 395.2198 .

2.3.3. Euphorin C (3)

Amorphous white powder; [α] + 21.0 (*c* 0.3, CH_2Cl_2); IR (KBr) ν_{max} cm^{-1}: 3420, 2926, 2872, 1729, 1453, 1372, 1204, 1043, 735; ^{13}C NMR (100 MHz, $CDCl_3$) data and ^{1}H NMR (400 MHz, $CDCl_3$), see Tables 1 and 2; ESIMS *m/z* 473 $[M+Na]^+$; HRESIMS *m/z* 473.2150 $[M+Na]^+$, calcd for $C_{24}H_{34}NaO_8$, 473.2151.

2.3.4. Euphorin D (4)

Amorphous white powder; [α] − 21.4 (*c* 0.4, CH_2Cl_2); IR (KBr) ν_{max} cm^{-1}: 3510, 2956, 2925, 1732, 1707, 1452, 1371, 1234, 736; ^{13}C NMR (100 MHz, $CDCl_3$) data and ^{1}H NMR (400 MHz, $CDCl_3$), see Tables 1 and 2; ESIMS *m/z* 577 $[M+Na]^+$; HRESIMS *m/z* 577.2412 $[M + Na]^+$ (calcd for $C_{31}H_{38}NaO_9$, 577.2414).

2.3.5. Euphorin E (5)

Colorless oil; [α] − 47.5 (*c* 0.3, CH_2Cl_2); IR (KBr) ν_{max} cm^{-1}: 3496, 2957, 2928, 1732, 1703, 1454, 1372, 1235, 734; ^{13}C NMR (100 MHz, $CDCl_3$) data and ^{1}H NMR (400 MHz, $CDCl_3$), see Tables 1 and 2; ESIMS *m/z* 555 $[M+Na]^+$; HRESIMS *m/z* 555.2570 $[M+Na]^+$, calcd for $C_{29}H_{40}NaO_9$, 555.2570.

2.4. Computational analysis

According to the relative configuration of every compound deduced from NOESY spectrum and Chem3D modeling, systematic conformational searches were performed firstly using MOE software and appropriate conformers were selected for geometry optimizations. Geometry optimizations and re-optimizations on the B3LYP/6–31 + G(d,p) level

Table 1
^{13}C NMR data for compounds **1–5** (δ in ppm, 100 MHz, in $CDCl_3$).

Position	**1**		**2**		Position		**3**		**4**		**5**	
1	37.1	CH_2	37.7	CH_2	1		31.6	CH_2	31.5	CH_2	31.5	CH_2
2	34.7	CH_2	34.8	CH_2	2		29.6	CH	32.2	CH	32.2	CH
3	212.3	C	212.7	C	3		77.7	CH	81.3	CH	81.3	CH
4	51.8	C	52.0	C	4		71.4	C	71.7	C	71.7	C
5	56.8	CH	57.0	CH	5		116.5	CH	116.9	CH	116.6	CH
6	20.0	CH_2	20.1	CH_2	6		141.4	C	141.1	C	141.3	C
7	30.7	CH_2	31.5	CH_2	7		78.1	CH	76.2	CH	76.2	CH
8	47.2	C	47.6	C	8		71.3	CH	74.8	CH	74.0	CH
9	51.1	CH	51.9	CH	9		27.5	CH	23.5	CH	23.6	CH
10	37.6	C	47.6	C	10		18.4	C	19.3	C	19.1	C
11	25.5	CH_2	28.1	CH_2	11		31.0	CH	31.0	CH	30.9	CH
12	44.7	CH	38.3	CH	12		70.9	CH	70.8	CH	70.8	CH
13	75.0	CH	44.5	CH_2	13		43.1	CH	43.4	CH	43.4	CH
14	217.8	C	216.3	C	14		207.8	C	207.3	C	207.4	C
15	43.5	CH_2	42.5	CH_2	15		73.8	C	70.7	C	70.6	C
16	142.0	C	146.8	C	16		17.0	CH_3	16.4	CH_3	16.4	CH_3
17	111.3	CH_2	107.3	CH_2	17		17.9	CH_3	17.4	CH_3	17.3	CH_3
18	21.2	CH_3	20.8	CH_3	18		29.3	CH_3	29.2	CH_3	29.1	CH_3
19	65.8	CH_2	65.8	CH_2	19		16.5	CH_3	16.4	CH_3	16.4	CH_3
20	14.2	CH_3	13.4	CH_3	20		13.4	CH_3	13.3	CH_3	13.3	CH_3
OR-19	174.3	C	174.3	C	OR-3	1	170.8	C	170.8	C	170.8	C
	27.4	CH_2	27.4	CH_2		2	20.7	CH_3	20.9	CH_3	20.9	CH_3
	9.0	CH_3	9.0	CH_3	OR-8	1			166.1	C	167.5	C
						2			129.9	C	128.4	C
						3/7			129.7	CH	138.1	CH
						4/6			128.6	CH	14.5	CH_3
						5			133.3	CH	12.1	CH_3
					OR-12	1	170.7	C	170.5	C	170.5	C
						2	21.1	CH_3	21.1	CH_3	21.1	CH_3

were performed by Gaussian 09 package [38]. The time-dependent density functional theory (TDDFT) ECD calculations for the optimized conformers were carried out at the CAM-B3LYP/SVP level with a CPCM solvent model in acetonitrile, and the calculated ECD spectra of different conformers were simulated with a half bandwidth of ~ 0.4 eV. The ECD curves were extracted by SpecDis 1.62 software [39]. The overall ECD curves of all the compounds were weighted by Boltzmann distribution after UV correction.

2.5. Bioassay for NO inhibitory activities

The NO release in BV-2 cells was determined using the previous method [40,41]. Briefly, BV-2 cells were seeded in 96-well culture plates (5×10^4 cells/well) for 24 h at 37 °C, and incubated with or without 0.2 μg/mL of LPS (Sigma Chemical Co., St. Louis, MO, U.S.A.) in the absence or presence of the test compounds. 2-Methyl-2-thiopseudourea, sulfate (SMT) was used as a positive control. After 20 h, the

Table 2
^1H NMR data for compounds **1–5** (δ in ppm, J in Hz, 400 MHz, in $CDCl_3$).

Position	**1**	**2**	Position		**3**	**4**	**5**
1α	1.39 m	1.34 m	1α		2.82 dd (15.0, 9.2)	2.13 m	2.13 m
1β	1.93 m	1.89 m	1β		1.68 d (15.2)	2.09 m	2.08 m
2α	2.37 m	2.33 m	2		2.58 m	1.88 m	1.83 m
2β	2.74 m	2.74 m	3		5.21 d (8.4)	5.10 d (8.3)	5.09 d (8.3)
5	1.40 brd (12.6)	1.36 dd (12.7, 2.9)	5		5.76 s	5.89 s	5.84 s
6α	1.54 m	1.60 m	7		4.22 s	4.37 s	4.25 s
6β	1.60 m	1.70 m	8		3.46 dd (10.3, 1.9)	4.76 d (10.7)	4.56 d (10.7)
7α	0.93 m	0.91 m	9		1.26 m	1.56 t (10.3)	1.47 t (9.4)
7β	2.42 m	2.36 m	11		1.06 m	2.18 m	2.12 m
9	1.63 m[b]	1.61 m[b]	12		4.87 dd (11.0, 3.9)	4.92 dd (11.2, 3.8)	4.87 dd (11.1, 3.8)
11α	2.06 m	1.68 m	13		2.93 m	2.95 m	2.91 m
11β	1.75 m	1.94 m	16		0.91 d (7.4)	1.06 s	1.07 s
12	2.82 m	2.74 m	17		1.99 s	2.08 s	2.04 s
13α	3.90 d (2.8)	2.33 m[b]	18		1.10 s	1.14 s	1.09 s
13β		2.24 m[b]	19		1.09 s	0.85 s	0.83 s
15a	2.32 m	2.32 m	20		1.06 d (7.3)	1.08 d (13.1)	1.05 s
15b	2.32 m	2.21 m	OR-3[a]	2	2.12 s	2.10 s	2.10 s
17a	5.03 s	4.90 s	OR-8[a]	3/7		8.05 d (7.3)	6.90 q (7.0)
17b	4.87 s	4.69 s		4/6		7.48 t (7.3)	1.81 d (7.0)
18	1.16 s	1.15 s		5		7.59 t (7.3)	1.84 s
19a	4.59 d (11.4)	4.63 d (11.3)	OR-12[a]	2	2.12 s	2.10 s	2.10 s
19b	3.84 d (11.4)	3.84 d (11.3)					
20	0.93 s	0.97 s					
OR-19[a]	2.26 q (7.5)	2.26 q (7.6)					
	1.09 t (7.5)	1.08 t (7.6)					

[a] The number with the superscript indicates the location of the substituent group in the parent skeleton.
[b] Signals are in overlapped regions of the spectra, and the multiplicities could not be discerned.

cell supernatants were collected and reacted with 50 μL of Griess reagent [1:1 mixture of 0.1% *N*-(1-naphtyl)ethylenediamine in H_2O and 1% sulfanilamide in 5% phosphoric acid] in a 96 well plate and the absorbance was read on a Multiskan MK3 microplate reader (Thermo Fisher Scientific Inc., Waltham, MA, USA). The amount of nitrite was calculated using a standard curve of known nitrite concentration versus absorbance at 550 nm. The IC_{50} values were determined using the software SPSS11.5 from the corresponding experiments performed in triplicate.

2.6. Molecular docking studies

Molecular docking simulations were performed using the software AutoDock Vina along with AutoDock Tools (ADT 1.5.6) using the hybrid Lamarckian Genetic Algorithm (LGA) [40,41]. The three dimensional (3D) crystal structures of iNOS (PDB code, 3E6T) and COX-2 (PDB code, 1PXX) were obtained from the RCSB Protein Data Bank, which resolution was 2.5 Å [42]. The standard 3D structures (PDB format) of selected compounds for molecular docking were constructed by chem3D Pro 14.0 software, whose configurations were determined by their NOESY spectra and Chem3D modeling. The cubic grid box of 20 Å size (x, y, z) with a spacing of 1.000 Å and grid maps were built. All of the other parameters were used according to default settings of AutoDock Vina. Results differing by less than 2.0 Å in positional root mean-square deviation (RMSD) were clustered together, and the results of the most favorable free energy of binding were chosen as the resultant complex structures.

2.7. Western blotting analysis

BV-2 cells were seeded in 12-well plates at the density of 3×10^5 cells/well for 24 h. Then, the cells were pretreated with the test compound for 30 min and stimulated with LPS (0.2 μg/mL) for 24 h. The cells were washed with cold PBS twice and collected, then the lysis buffer was added into cells and the lysates were centrifuged at 10,000 rpm for 10 min. The total proteins were acquired from the supernatants and the protein concentration was determined by the BCA protein assay kit. (Solarbio, Beijing, People's Republic of China). Approximate 20 μg protein were used and subjected to electrophoresis analysis of 10% sodium dodecyl sulphate-polyacrylamide gel electrophoresis (SDS-PAGE). After transferring to PVDF membranes, the membranes were blocked in 15% skim milk for 2 h at room temperature and incubated with primary antibodies (iNOS and COX-2, diluted 1:1000 in skim milk) overnight at 4 ℃. After being washed with TBST for 30 min, the membranes were incubated secondary antibody (diluted 1: 5000 in 5% skim milk) for 1 h at room temperature and then washed with TBST for 30 min. Lastly, the protein blots were developed using an ECL detection kit (Beyotime, Shanghai, People's Republic of China). *β*-Actin protein was used as internal reference. Each band was quantified by Image-J software.

3. Results and discussion

3.1. Structure elucidation

Compound **1** was obtained as a colorless oil. The molecular formula of $C_{23}H_{32}O_5$ for **1** was derived from the HRESIMS $[M+Na]^+$ ion at *m/z* 411.2145 (calcd for $C_{23}H_{32}NaO_5$, 411.2147) and the NMR data (Tables 1 and 2). The ^1H NMR spectrum of **1** displayed characteristic signals attributable to two aliphatic methyl singlets (δ_H 1.16 and 0.93), a pair of olefinic protons of terminal double bond [δ_H 5.03 and 4.87 (each 1H, s)], a set of oxymethylene protons [δ_H 4.59 and 3.84 (each 1H, d, J = 11.4 Hz)], and one oxymethine proton [δ_H 3.90 (1H, d, J = 2.8 Hz)]. The ^{13}C NMR spectrum of **1** showed 23 resonances, one of which was indicative of an ester carbonyl (δ_C 174.3). This ester carbonyl (δ_C 174.3) and the methylene and methyl resonances (δ_C 27.4 and 9.0), together with the corresponding proton signals (Table 2), suggested the presence of a propionyloxy group. The remaining 20 carbons displayed in the ^{13}C NMR spectrum comprised two methyls, eight methylenes [one olefinic methylene (δ_C 111.3)], four methines [one oxygenated methine (δ_C 75.0)], and six quaternary carbons [two ketone carbonyls (δ_C 212.3 and 217.8) and one olefinic carbon (δ_C 142.0)] based on the DEPT and HMQC spectra (Table 1). These NMR spectroscopic features indicated compound **1** to be a diterpenoid with a propionyloxy group [17,18,43]. The following HMBC and ^1H–^1H COSY experiments were performed to elucidate this diterpenoid scaffold. From the HMBC spectrum, the long range couplings of H_3-18 to C-3, C-4, C-5, and C-19, H_2-19 to C-3, C-4, C-5, and C-18, H_3-20 to C-1, C-5, C-9, and C-10, H-5 to C-1, C-3, C-4, C-6, C-7, C-9, and C-10, H-9 to C-1, C-5, C-7, C-8, C-10, and C-20, and H_2-2 to C-1, C-3, C-4, and C-10, as well as the ^1H–^1H COSY correlations (Fig. 2), revealed the presence of two fused six-membered rings A and B. In addition, another six-membered ring consisting of C-8, C-9, C-11, C-12, C-15, and C-16 was also inferred from the ^1H–^1H COSY couplings of H-9/H_2-11/H-12 and the HMBC correlations of H-12 to C-9, C-11, and C-15 − C-17, and H_2-17 with C-12, C-15, and C-16 (Fig. 2). Correspondingly, the ketone carbonyl, oxygenated, and olefinic carbon signals at δ_C 212.3 (C-3), 65.8 (C-19), 142.0 (C-16), and 111.3 (C-17) as well as the other carbon signals of the three six-membered rings were assigned, respectively, via interpretation of the 2D NMR data. There were two carbon signals left including one ketone carbonyl (δ_C 217.8) and one oxymethine (δ_C 75.0). The two signals were attributed to C-13 (δ_C 75.0) and C-14 (δ_C 217.8) to connect the bridgehead carbons C-8 and C-12 and constitute a bridge ring, which was supported by the ^1H–^1H COSY correlations of H-12/H-13 and the corresponding HMBC correlations as illustrated in Fig. 2. All of the above NMR data analysis pointed toward an atisane-type diterpenoid scaffold for **1** as depicted in Fig. 1 [17,18].

After defining the 2D structure, NOESY interactions and Chem3D simulations enabled the stereochemistry of compound **1** to be assigned. The NOESY spectrum of **1** showed the proton interactions of H_3-18/H-5, H_3-18/H-6*β*, H_2-19/H_3-20, H_2-19/H-2*α*, H_2-19/H-6*α*, H_3-20/H-1*α*, H_3-20/H-2*α*, H_3-20/H-6*α*, H_3-20/H-11*α*, H_3-20/H-13, H-5/H-9, H-9/H-15b, and H-11*α*/H-13 (Fig. 3). According to these NOESY correlations, along with Chem3D modeling, the molecular conformation of **1** was disclosed as illustrated in Fig. 3. In this molecular arrangement of **1**, two six-membered rings A and B existed in a twist chair and a chair conformation and were trans-fused with H-5 in a *β*-axial position and C-20 in an *α*-axial position, ring B and the six-membered ring consisting of C-8, C-9, C-11, C-12, C-15, and C-16, shared C-8 and C-9 and were also trans-fused with H-9 *β*-oriented and the C-13 − C-14 bridge connection unit on the *α*-face, and the C-19 occupied an *α*-axial position. The final confirmation of stereochemistry of **1** was accomplished by comparing experimental and calculated ECD data, an applicable method to solve the absolute configuration of natural products [44]. After systematic conformational search, geometry optimizations, and TDDFT calculations, the ECD spectra were extracted using SpecDis 1.62 software. The calculated ECD spectrum of **1** (Fig. 5A) accorded with the experimental data closely, pointing to an absolute configuration of 4*R*, 5*S*, 8*S*, 9*S*, 10*S*, 12*S*, and 13*R* for **1**. Compound **1** was therefore elucidated and has been given a trivial name euphorin A.

Compound **2**, a colorless oil, gave a molecular formula of $C_{23}H_{32}O_4$ as determined from the HRESIMS (*m/z* 395.2197 $[M+Na]^+$, calcd for $C_{23}H_{32}NaO_4$, 395.2198). From the ^1H and ^{13}C NMR spectra, the ester carbonyl, methylene, and methyl carbons at δ_C 174.3, 27.4, and 9.0, along with the corresponding proton signals (Table 2) were indicative of a propionyloxy group, which was the same as that of compound **1**. Excluding the signals for the propionyloxy group, the ^1H and ^{13}C NMR spectra showed similar proton and carbon signals to those of compound **1**, which suggested compound **2** should also be an *ent*-atisane type diterpenoid related structurally to **1**. Further comparison of the chemical shifts of skeletal carbons of **1** and **2** indicated that one more aliphatic methylene appeared in **2**, and the oxymethine [δ_C 75.0 (C-13)] present

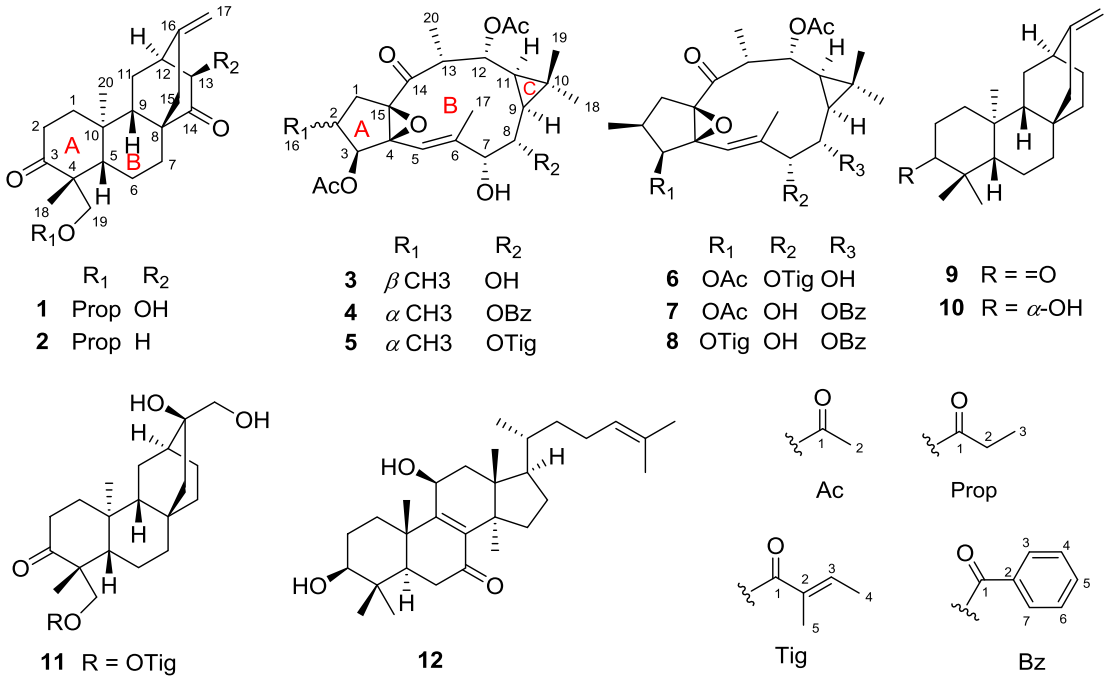

Fig. 1. Chemical structures of compounds **1–12**.

in **1** was not observed from the ^{13}C NMR spectrum of **2**, implying the oxymethine [δ_C 75.0 (C-13)] in **1** was replaced by the aliphatic methylene [δ_C 44.5 (C-13)] in **2**. This deduction was concluded by the following 2D NMR experiments, and the skeletal proton and carbon signals were assigned via interpretation of the 2D NMR data. It was found that the only structural difference between compounds **2** and **1** was the C-13 hydroxy group in **1** was replaced by a proton. A NOESY experiment disclosed that compound **2** had the same skeletal conformation as that of **1**. After defining the relative configuration, an experimental ECD spectrum of **2** was recorded, which was almost identical to that of **1** (Fig. 5B). Based on the same relative configuration and the identical ECD spectra of compounds **1** and **2**, the absolute configuration of **2** was assigned as 4*R*, 5*S*, 8*S*, 9*S*, 10*S*, and 12*R*. Compound **2** was thus elucidated to be an *ent*-atisane diterpenoid with a propionyloxy group attached at C-19 and designated as a trivial name euphorin B.

The molecular formula of compound **3** was determined as $C_{24}H_{34}O_8$ from the ^{13}C NMR data and HRESIMS (*m/z* 473.2150 $[M+Na]^+$, calcd for $C_{24}H_{34}NaO_8$, 473.2151), which indicated 11 indices of hydrogen deficiency. From its ^{1}H and ^{13}C NMR spectra, two sets of carbonyl signals at δ_C 170.8 and 170.7, together with the methyl singlets at δ_H 2.12 and 2.12, were representative of two acetyloxy groups. Excluding

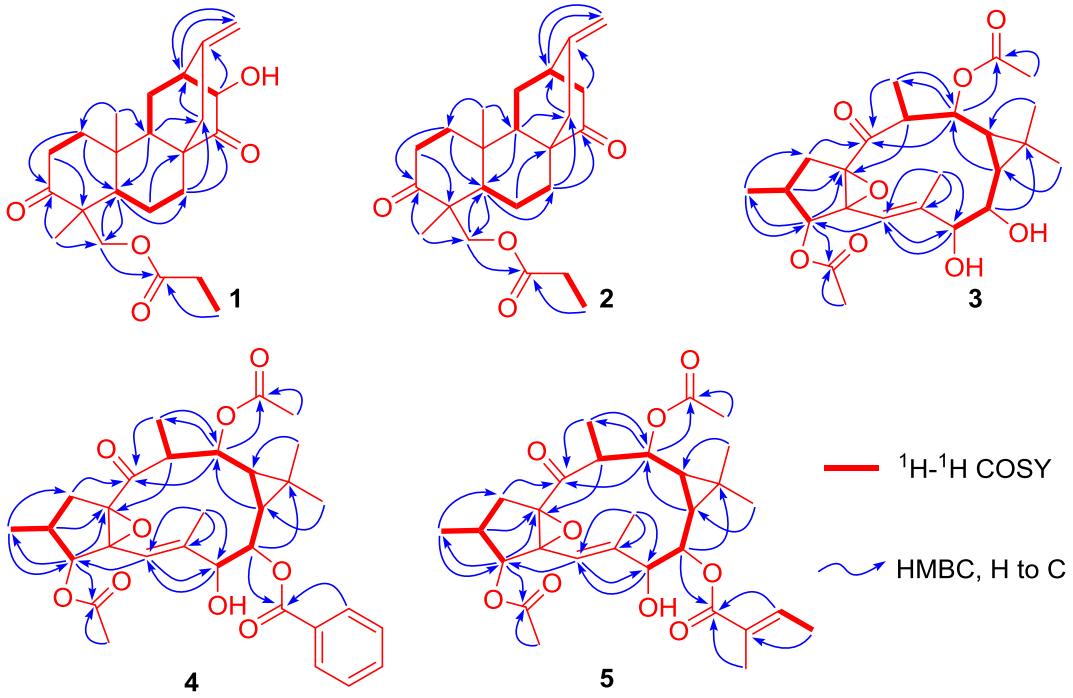

Fig. 2. ^{1}H–^{1}H COSY and key HMBC correlations of compounds **1–5**.

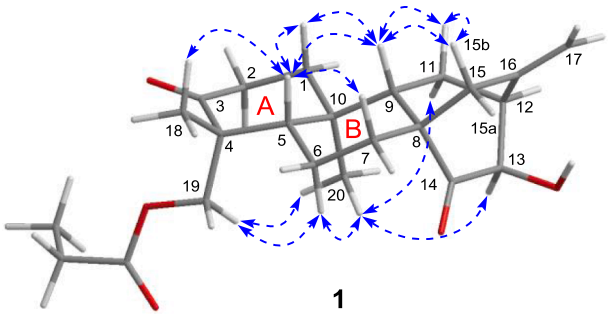

Fig. 3. Conformation and key NOESY correlations of compound **1**.

Table 3
IC_{50} values of compounds **1–12** inhibiting NO production in BV-2 cells.

Compound	IC_{50} (μM)	Compound	IC_{50} (μM)
1	35.8 ± 3.2	**8**	14.9 ± 2.3
2	41.4 ± 1.4	**9**	71.0 ± 4.8
3	> 100	**10**	31.6 ± 0.7
4	32.0 ± 2.9	**11**	56.6 ± 1.4
5	40.7 ± 2.7	**12**	> 30
6	49.2 ± 2.2	SMT[a]	4.2 ± 0.2
7	14.5 ± 0.4		

[a] SMT(2-Methyl-2-thiopseudourea, sulfate) was used as a positive control. Data are presented based on three experiments.

the four signals for the substituent groups, the remaining 20 carbons were sorted as five methyls, one methylene, nine methines [four oxymethines (δ_C 77.7, 78.1, 71.3, and 70.9) and one olefinic methine (δ_C 116.5)], and five quaternary carbons [one ketone carbonyl (δ_C 207.8), one olefinic carbon (δ_C 141.4), and two oxygenated tertiary carbons (δ_C 71.4 and 73.8)] based on the DEPT and HMQC spectra. These spectroscopic features indicated compound **1** to be a diterpenoid carrying two acetyloxy residues. The following HMBC and ^{1}H–^{1}H COSY experiments enabled the diterpenoid skeleton to be elucidated. The HMBC correlations of H_2-1 to C-2 − C-4, C-15, and C-16, H_3-16 to C-1 − C-3, H-3 to C-1, C-2, C-4, C-15, and C-16, revealed the presence of five-membered ring A with a methyl group attached at C-2 (Fig. 2). Another three-membered ring C with two methyl groups (Me-18 and Me-19) attached at C-10 was also inferred according to the typically upfield aliphatic quaternary carbon signal at δ_C 18.4 (C-10) and the HMBC couplings of H_3-18(19) to C-9 − C-11, as well as the ^{1}H–^{1}H COSY correlation of H-9/H-11. In addition to the above rings A and C, another macroring consisting of C-4 − C-9 and C-11 − C-15 was deduced from the HMBC and ^{1}H–^{1}H COSY correlations as shown in Fig. 2. The fusion of rings A/B and B/C by sharing C-4/C-15 (rings A/B) and C-9/C-11 (rings B/C) led to the establishment of a lathyrane-type diterpenoid scaffold. By interpretation of 1D and 2D NMR spectra, the carbonyl, oxygenated, and olefinic carbons at δ_C 207.8 (C-14), 77.7 (C-3), 71.4 (C-4), 78.1 (C-7), 71.3 (C-8), 70.9 (C-12), 73.8 (C-15), 116.5 (C-5), and 141.1 (C-6), as well as the other proton and carbon signals were assigned. There were two acyloxy groups left to be assigned in compound **3**, which were attributed to C-3 and C-12, respectively, by the HMBC correlations of H-3 and H-12 to the corresponding carbonyl carbons of the acetyloxy groups. The above analysis led to the establishment of a planar structure for **3**. However, the molecular formula from this planar structure was inconsistent with the HRESIMS data, implying the presence of one more ring. The total indices of hydrogen deficiency and the chemical shifts of C-4 and C-15 suggested a 4,15-epoxy moiety [45].

The relative configuration of **3** was assigned by a NOESY experiment, in which H-2, H-3, H-7, H-8, H-9, H-11, H-12, H-13, H_3-18, and H_3-19 were determined as *α*-, *α*-, *β*-, *β*-, *α*-, *α*-, *β*-, *β*-, *α*-, and *β*-oriented, respectively, on the basis of NOESY correlations of H-1*β*/H_3-16, H-2/H-3, H-3/H-5, H-5/H-7, H_3-17/H-7, H_3-17/H-8, H_3-19/H-8, H_3-19/H-12, H_3-19/H-13, H-12/H-13, H_3-18/H-9, and H_3-18/H-11 (Fig. 4). While, the coupling constant of $J_{2,3}$ = 8.4 Hz and the chemical shifts of H_2-1 also supported *α*-orientations for H-2 and H-3 protons [45–47]. The Δ^5 double bond was assigned as *E*-geometry from the NOESY correlation of H-5/H-7. The 4,15-epoxy ring was proposed to be on the *β*-face, which was the same as those of known analogues based on their identical coupling patterns of the protons and chemical shifts of carbons in rings A and B [45–47]. There is an eleven-membered ring in compound **3**, which is flexible to produce so many conformations. Considering the numerous conformations of **3**, it is not feasible to use TDDFFT calculations to determine the absolute configuration. So, only the relative configuration of **3** was assigned and compound **3** was given a trivial name euphorin C.

Compound **4** (euphorin D) gave the molecular formula $C_{31}H_{38}O_9$ as determined from the HRESIMS and ^{13}C NMR data. From the ^{1}H and ^{13}C NMR spectra, two acetyloxy groups as present in compound **3** were deduced from the characteristic carbon and proton signals (Tables 1 and 2). In addition, a set of aromatic proton and carbon signals (Tables 1 and 2), together with the ester carbonyl at δ_C 166.1, were indicative of a benzoyloxy group. Excluding these signals for the three acyloxy groups, there were additional 20 carbons displayed in the ^{13}C NMR spectrum, indicating a diterpenoid skeleton for **4**. Comparison of chemical shifts of skeletal carbons in compounds **4** and **3** suggested two compounds shared the same scaffold. This deduction was concluded by the following DEPT, HMQC, HMBC, and ^{1}H–^{1}H COSY experiments, and the assignments of skeletal proton and carbon signals were accomplished via interpretation of the 2D NMR data. The HMBC correlations of H-3, H-8, and H-12 to the corresponding carbonyl carbons of acyloxy groups allowed the benzoyloxy and two acetyloxy groups assignable to C-8, C-3, and C-12, respectively. The planar structure of **4** was established based on the above spectroscopic data analysis, which was the same as that of the known compound 3,12-diacetyl-8-benzoylingol reported in the liaterature [48,49]. However, the NMR data of two compounds seemed to be a little different, implying configurational differences. Upon detailed comparison of their NMR data, it was found that the chemical shift of C-2 in compound **4** shifted downfield by about 3 ppm [δ_C 32.2 (C-2) in compound **4**; δ_C 29.7 (C-2) in 3,12-diacetyl-8-benzoylingol], and the chemical shifts of H_2-1 [δ_H 2.09 and 2.13 (H_2-1) in compound **4**; δ_H 1.69 and 2.83 (H_2-1) in 3,12-diacetyl-8-benzoylingol] varied distinctly. These facts suggested a *β*-orientation of H-2 in

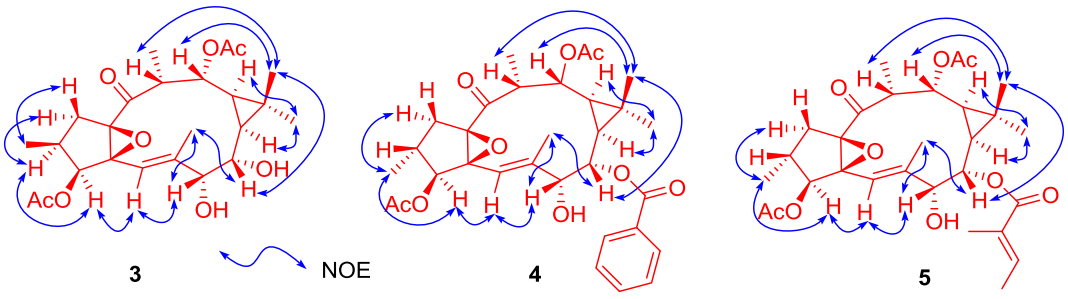

Fig. 4. Key NOESY correlations and of compounds **3–5**.

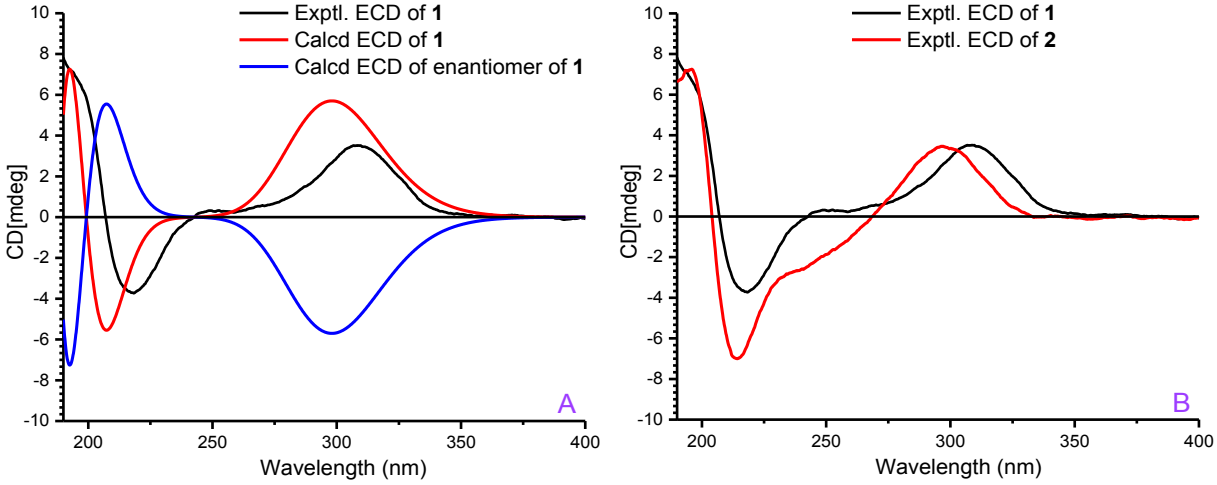

Fig. 5. Calculated and/or experimental ECD spectra for compounds **1** (A) and **2** (B) in acetonitrile.

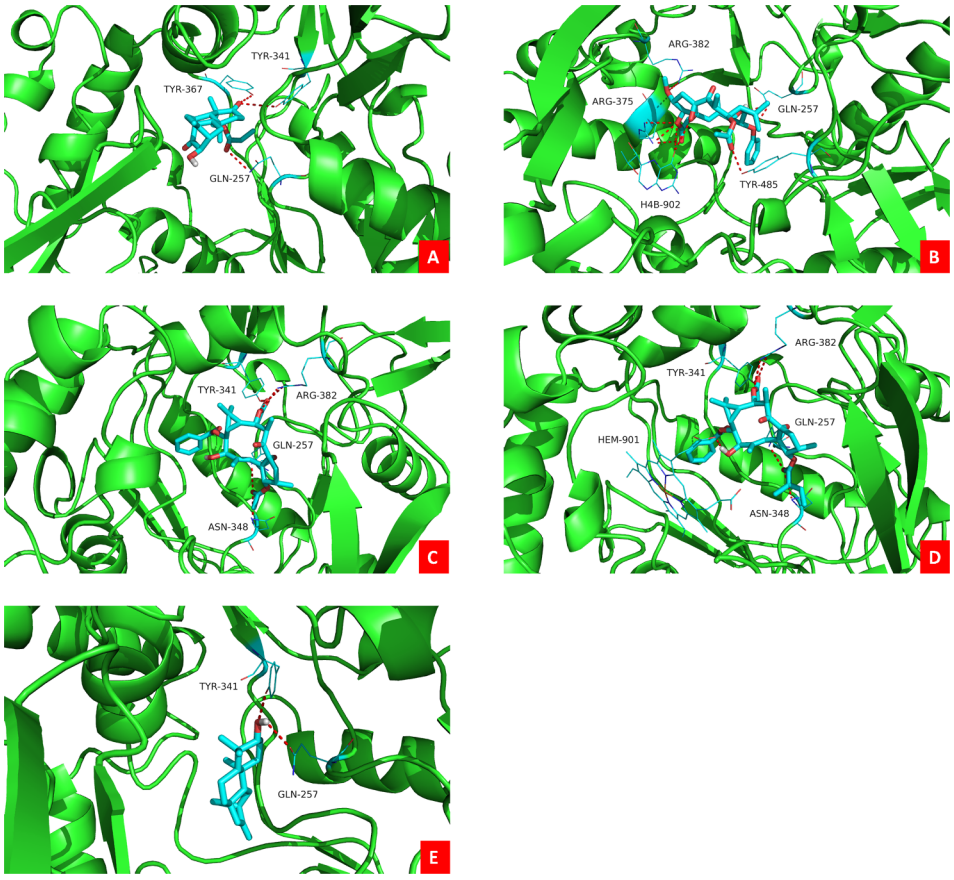

Fig. 6. Molecular docking results of some bioactive compounds with iNOS protein. Molecular docking simulations obtained at lowest energy conformation, highlighting potential hydrogen contacts of compounds **1** (A), **4** (B), **7** (C), **8** (D), and **10** (E), respectively (Colored by atom: carbon is cyan; nitrogen is blue; oxygen is red; hydrogen is gray; sulfur is orange). For clarity, only interacting residues are labeled. Hydrogen bonding interactions are shown by dashes. These figures were created by PyMOL.

4 instead of an *α*-orientation of H-2 in 3,12-diacetyl-8-benzoylingol [48,49]. The subsequent NOESY experiment confirmed the above configuration deduction and enabled H-3, H-7, H-8, H-9, H-11, H-12, and H-13 to be assigned as *α*-, *β*-, *β*-, *α*-, *α*-, *β*-, and *β*-oriented, respectively. As in the case of **3**, the presence of eleven-membered ring in **4** led to numerous conformations for compound **4**, and it is unsuitable to determine the absolute configuration using TDDFT ECD calculations.

Analysis of the ^{1}H and ^{13}C NMR spectra indicated that compound **5** should be a diterpenoid with two acetyloxy groups [δ_C 170.8, 170.5, 21.1, and 20.9; δ_H 2.10 (6H, s)] and one tigloyloxy group [δ_C 167.5, 138.1, 128.4, 14.5 and 12.1; δ_H 6.90 (1H, q, J = 7.0 Hz), 1.84 (3H, s), and 1.81 (3H, d, J = 7.0 Hz)]. The chemical shifts of skeletal carbons of **5** were almost identical to those of compound **4**, suggesting two compounds shared the same scaffold. This skeleton of lathyrane-type diterpenoid and the tigloylxoy group in compound **5** were further confirmed by comprehensive analysis of 1D and 2D NMR data. The locations of acyloxy groups were determined from the HMBC spectrum. The HMBC correlations of H-3, H-8, and H-12 to the corresponding carbonyls of the acyloxy groups allowed the tigloyloxy and two acetyloxy groups assignable to C-8, C-3, and C-12, respectively. The above analysis led to the establishment of a planar structure for compound **5**, which was the same as that of the reported compound 3,12-di-*O*-acetyl-8-*O*-tigloylingol [50-53]. However, comparison of their NMR data indicated the distinct differences of chemical shifts, especially for H_2-1 [δ_H 2.08 and 2.13 (each 1H) in compound **5**; δ_C 2.80 and 1.65 (each 1H) in 3,12-di-*O*-acetyl-8-*O*-tigloylingol] and C-2 [δ_C 32.2 in compound **5**;

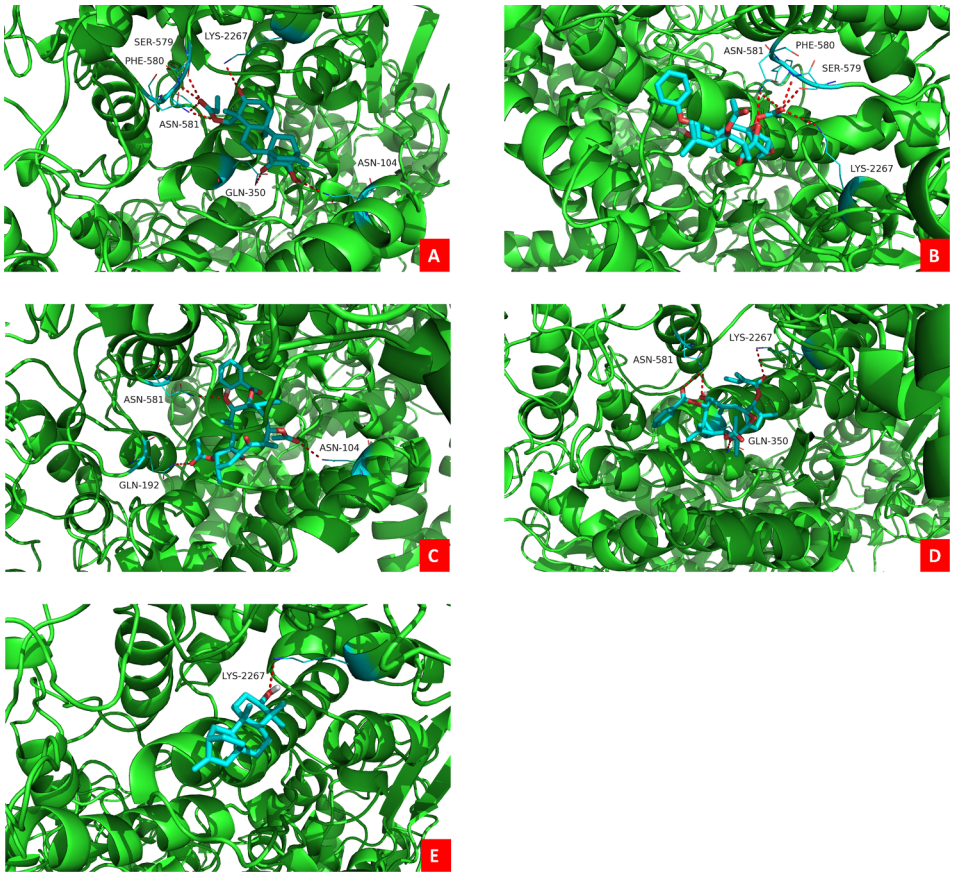

Fig. 7. Molecular docking results of some bioactive compounds with COX-2 protein. Molecular docking simulations obtained at lowest energy conformation, highlighting potential hydrogen contacts of compounds **1** (A), **4** (B), **7** (C), **8** (D), and **10** (E), respectively (Colored by atom: carbon is cyan; nitrogen is blue; oxygen is red; hydrogen is gray; sulfur is orange). For clarity, only interacting residues are labeled. Hydrogen bonding interactions are shown by dashes. These figures were created by PyMOL.

Table 4
Logarithms of free binding energies (FBE, kcal/mol) of compounds to the active cavities of iNOS (PDB code: 3E6T) and targeting residues of the binding site located on the mobile flap.

Compound	−Log (FBE)	Targeting residues
1	−8.6	TYR-341 TYR-367 GLN-257
4	−9.1	ARG-382 ARG-375 GLN-257 H4B-902 TYR-485
7	−10.9	ARG-382 TYR-341 GLN-257 ASN-348
8	−11.1	ARG-382 TYR-341 GLN-257 ASN-348 HEM-901
10	−8.4	TYR-341 GLN-257

Table 5
Logarithms of free binding energies (FBE, kcal/mol) of compounds to the active cavities of COX-2 (PDB code: 1PXX) and targeting residues of the binding site located on the mobile flap.

Compound	−Log (FBE)	Targeting residues
1	−7.9	SER-579 PHE-580 LYS-2267 ASN-581 GLN-350 ASN-104
4	−8.2	SER-579 PHE-580 LYS-2267 ASN-581
7	−8.1	ASN-581 ASN-104 GLN-192
8	−8.1	LYS-2267 ASN-581 GLN-350
10	−7.8	LYS-2267

δ_C 29.7 in 3,12-di-*O*-acetyl-8-*O*-tigloylingol] [51], suggesting compound **5** should be a stereoisomer of the known compound 3,12-di-*O*-acetyl-8-*O*-tigloylingol. The following NOESY data analysis disclosed that compound **5** had the same skeletal configuration as compound **4** and H-2, H-3, H-7, H-8, H-9, H-11, H-12, and H-13 were determined as *β*-, *α*-, *β*-, *β*-, *α*-, *α*-, *β*-, and *β*-oriented, respectively. It was found that the only configurational difference is the change of Me-16 from a *β*-orientation in 3,12-di-*O*-acetyl-8-*O*-tigloyl-ingol to an *α*-orientation in **5**. Compound **5** was thus characterized and given a trivial name euphorin E.

In addition to five new diterpenoids, seven known terpenoids were also isolated from the stems of *E. antiquorum*. Using 1D (^{1}H and ^{13}C) and/or 2D NMR experiments and comparing their NMR data with those reported in the literature, the known compounds were identified as 3,12-*O*-diacetyl-7-*O*-[(*E*)-2-methyl-2-butenoyl]-8,12-diepjing-ol (**6**) [54], 3,12-diacetyl-8-benzoylingol (**7**) [48], 12-*O*-acetyl-8-*O*-benzoylingol 3-tiglate (**8**) [47]. *ent*-3,14-dioxo-16-atisene (**9**) [55], *ent*-(3*α*,5*β*,8*α*,9*β*,10*α*,12*α*)-3-hydroxyatis-16-en-14-one (**10**) [56], eurifoloid R (**11**) [57], and (3*β*,11*β*)-3,11-dihydroxylanosta-8,24-dien-7-one (**12**) [58].

3.2. Bioassay for anti-inflammatory activities

According to traditional efficacy of *E. antiquorum*, the obtained diterpenoids were subjected to anti-inflammatory assay using the previous method, in which the amount of NO is regarded as an indicator of inflammatory response [6,59]. After treatment with different concentrations of these diterpenoids, the amount of NO was measured and the IC_{50} values of NO inhibitory effects were calculated (Table 3). The bioassay results disclosed that all the diterpenoids inhibited NO production in LPS-induced murine microglial BV-2 cells. Compared to the positive control, 2-methyl-2-thiopseudourea, sulfate (SMT) with an IC_{50} value of 4.2 μM, compounds **1**, **4**, **7**, **8**, and **10** (IC_{50} < 40 μM) seem to be more active among the tested compounds. The cytotoxic test (MTT assay) showed that all of the isolates had no impact on BV-2 cell survival at their effective dose range (data not shown).

3.3. Interactions of bioactive compounds with iNOS/COX-2 protein

NO is a sign of inflammatory response, and excessive NO in tissues means a high-expression of the crucial proteins iNOS and COX-2

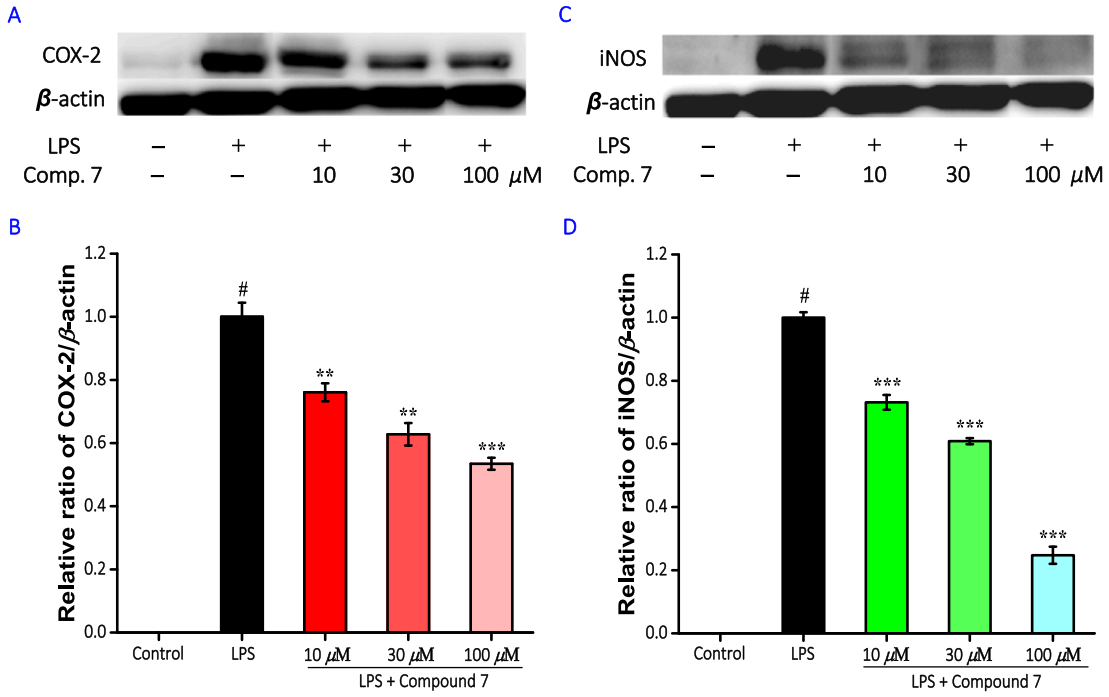

Fig. 8. Effects of compound **7** on LPS-induced iNOS and COX-2 protein expressions in BV-2 cells. BV-2 cells were pre-treated with compound **7** for 30 min, then stimulated by LPS (0.2 μg/ml) for 24 h, and Western blotting analysis was performed. (A) Western blotting results of COX-2 protein levels. (B) Quantitative analysis of COX-2 protein expression. (C) Western blotting results of iNOS protein levels. (D) Quantitative analysis of iNOS protein expression. β-Actin protein was used as internal reference. $^{\#}p < 0.001$ compared with LPS-untreated cells, $^{***}p < 0.001$, $^{**}p < 0.01$, compared with LPS-stimulated cells. Data were obtained by at least three independent experiments.

[60,61], of which the former catalyze to produce NO in the inflammatory signaling pathway [4]. It has reported that the bindings of iNOS/COX-2 with some small molecules can arrest inflammatory response and inhibit the generation of excessive downstream inflammatory mediators [62]. To explore the possible mechanism of NO inhibition, the binding interactions of bioactive compounds with iNOS/COX-2 were investigated. The more bioactive compounds (**1**, **4**, **7**, **8**, and **10**) with significant NO inhibitory effects (IC_{50} < 40 μM) were subjected to molecular docking. Results from molecular docking studies revealed that compounds **1**, **4**, **7**, **8**, and **10** had strong interactions with the iNOS/COX-2 protein (Figs. 6 and 7) and the binding residues and the logarithms of free binding energies were collated in Tables 4 and 5.

3.4. Effects on iNOS/COX-2 protein expressions

Molecular docking studies disclosed that the possible anti-inflammatory mechanism is the bindings of iNOS/COX-2 with bioactive diterpenoids, which means the reduction of free iNOS and COX-2 proteins. To confirm whether the protein expression levels of iNOS/COX-2 are decreased, Western blotting experiments were performed. As seen in Fig. 8, after stimulation with LPS for 24 h, the expressions of iNOS and COX-2 were increased remarkably. However, with the treatment of the selected compound **7**, iNOS and COX-2 were decreased significantly. These experiments, along with the docking results, indicated that compound **7** may exert its anti-inflammatory effects by down-regulating iNOS and COX-2 protein levels.

4. Conclusion

The current phytochemical investigation of *E. antiquorum* led to the isolation of 12 compounds including five new diterpnoids (**1–5**) from the stems of *E. antiquorum*. The structures were elucidated on the basis of extensive 1D and 2D NMR spectroscopic data analysis, and the ECD calculations were used to determine the absolute configuration. In the following anti-inflammatory assay, compounds **1**, **4**, **7**, **8**, and **10** exerted more inhibition against NO production with IC_{50} values less than 40 μM. The molecular docking studies revealed that some bioactive diterpenoids can bind with the crucial proteins iNOS and COX-2 of inflammatory signaling pathway to reduce the amount of free iNOS/COX-2 protein. The further Western blotting experiments confirmed the down-regulation of iNOS and COX-2 in BV-2 cells treated with compound **7**. The results from molecular docking and Western blotting revealed the preliminary anti-inflammatory mechanism. All the research conducted on the chemical constituents and the anti-inflammatory effects disclosed that the plant *E. antiquorum* or its bioactive components are potential useful as a folk medicine for the treatment of inflammation and related diseases.

Declaration of Competing Interest

The authors declared that there is no conflict of interest.

Acknowledgments

This research was financially supported by the National Natural Science Foundation of China (Nos. U1703107, U1801288, and 21665013), the National Key Research and Development Program of China (No. 2018YFA0507204), Hundred Young Academic Leaders Program of Nankai University, State Key Laboratory for Chemistry and Molecular Engineering of Medicinal Resources (Guangxi Normal University, No. CMEMR2018-B02), the Fundamental Research Funds for the Central Universities, Nankai University (Nos. 63191142 and 63191731), and the Natural Science Foundation of Tianjin (No. 16JCQNJC13500).

Appendix A. Supplementary material

Supplementary data to this article can be found online at https://doi.org/10.1016/j.bioorg.2019.103237.

References

[1] G.R. Geovanini, P. Libby, Clin. Sci. (Lond). 132 (2018) 1243–1252.
[2] S. Purkayastha, D.S. Cai, Mol. Metab. 2 (2013) 356–363.
[3] E. Lontchi-Yimagou, E. Sobngwi, T.E. Matsha, A.P. Kengne, Curr. Diab. Rep. 13 (2013) 435–444.
[4] H.S. Lim, Y.J. Kim, B.Y. Kim, G. Park, S.J. Jeong, Front Pharmacol. 9 (2018) 462–475.
[5] Z.Y. Zhong, E. Sanchez-Lopez, M. Karin, Cell. 166 (2016) 288–298.
[6] M.E. Kim, I. Jung, J.Y. Na, Y. Lee, J. Lee, J.S. Lee, J.S. Lee, Molecules. 23 (2018) 3196–3209.
[7] Editorial Committee of the Flora of China, Chinese Academy of Sciences. Flora of China, Vol. 44 (3), Science Press, Beijing, 1997, pp. 26 – 27.
[8] M. Ernst, O.M. Grace, C.H. Saslis-Lagoudakis, N. Nilsson, H.T. Simonsen, N. Rønsted, J. Ethnopharmacol. 176 (2015) 90–101.
[9] Q.W. Shi, X.H. Su, H. Kiyota, Chem. Rev. 108 (2008) 4295–4327.
[10] A. Vasas, J. Hohmann, Chem. Rev. 114 (2014) 8579–8612.
[11] Z.L. Yu, Y.L. Wei, X.G. Tian, Q.L. Yan, Q.S. Yan, X.K. Huo, C. Wang, C.P. Sun, B.J. Zhang, X.C. Ma, Bioorg. Chem. 77 (2018) 471–477.
[12] R. Hu, J. Gao, R. Rozimamat, H.A. Aisa, Eur. J. Med. Chem. 146 (2018) 157–170.
[13] G. Krstic, M. Jadranin, N.M. Todorovic, M. Pesic, T. Stankovic, I.S. Aljancic, V.V. Tesevic, Phytochemistry 148 (2018) 104–112.
[14] A.H. Wang, X.G. Tian, Y.L. Cui, X.K. Huo, B.J. Zhang, S. Deng, L. Feng, X.C. Ma, J.M. Jia, C. Wang, Phytochemistry 146 (2018) 82–90.
[15] J. Bai, X.Y. Huang, Z.G. Liu, C. Gong, X.Y. Li, D.H. Li, H.M. Hua, L. Zhan, Fitoterapia 125 (2018) 235–239.
[16] Y. Wei, C. Wang, Z. Cheng, X. Tian, J. Jia, Y. Cui, L. Feng, C.P. Sun, B.J. Zhang, X.C. Ma, J. Nat. Prod. 80 (2017) 3218–3223.
[17] W.P. Wang, K. Jiang, P. Zhang, K.K. Shen, S.J. Qu, X.P. Yu, C.H. Tan, Phytochemistry 145 (2018) 93–102.
[18] S.L. Yan, Y.H. Li, X.Q. Chen, D. Liu, C.H. Chen, R.T. Li, Phytochemistry 145 (2018) 40–47.
[19] L.F. Nothias, S. Boutet-Mercey, X. Cachet, L.T.E. De, L. Laboureur, J.F. Gallard, P. Retailleau, A. Brunelle, P.C. Dorrestein, J. Costa, L.M. Bedova, F. Roussi, P. Leyssen, J. Alcami, M. Litaudon, D. Touboul, J. Nat. Prod. 80 (2017) 2620–2629.
[20] M.E. Flores-Giubi, M.J. Duran-Pena, J.M. Botubol-Ares, F. Escobar-Montano, D. Zorrilla, A.J. Macias-Sanchez, R. Hernandez-Galan, J. Nat. Prod. 80 (2017) 2161–2165.
[21] M. Esposito, L.F. Nothias, P. Retailleau, J. Costa, F. Roussi, J. Neyts, P. Leyssen, D. Touboul, M. Litaudon, J. Paolini, J. Nat. Prod. 80 (2017) 2051–2059.
[22] M.A. Reis, O.B. Ahmed, G. Spengler, J. Molnar, H. Lage, M.U. Ferreira, J. Nat. Prod. 80 (2017) 1411–1420.
[23] C.J. Wang, Q.L. Yan, Y.F. Ma, C.P. Sun, C.M. Chen, X.G. Tian, X.Y. Han, C. Wang, S. Deng, X.C. Ma, J. Nat. Prod. 80 (2017) 1248–1254.
[24] M. Esposito, S. Nim, L.F. Nothias, J.F. Gallard, M.K. Rawal, J. Costa, F. Roussi, R. Prasad, A. Di-Pietro, J. Paolini, M. Litaudon, J. Nat. Prod. 80 (2017) 479–487.
[25] S.N. Liu, D. Huang, S.L. Morris-Natschke, H. Ma, Z.H. Liu, N.P. Seeram, J. Xu, K.H. Lee, Q. Gu, Org. Lett. 18 (2016) 6132–6135.
[26] M. Esposito, L.F. Nothias, H. Nedev, J.F. Gallard, P. Leyssen, P. Retailleau, J. Costa, F. Roussi, B.I. Iorqa, J. Paolini, M. Litaudon, J. Nat. Prod. 79 (2016) 2873–2882.
[27] J.Y. Tsai, D. Redei, P. Forgo, Y. Li, A. Vasas, J. Hohmann, C.C. Wu, J. Nat. Prod. 79 (2016) 2658–2666.
[28] F. Dal-Piaz, M.B. Vera-Saltos, S. Franceschelli, G. Forte, S. Marzocco, T. Tuccinardi, G. Poli, S. Nejad-Ebrahimi, M. Hamburger, N. De-Tommasi, A. Braca, J. Nat. Prod. 79 (2016) 2681–2692.
[29] A. Vasas, P. Forgo, P. Orvos, L. Talosi, A. Csorba, G. Pinke, J. Hohmann, J. Nat. Prod. 79 (2016) 1990–2004.
[30] J.W. Lee, Q. Jin, H. Jang, D. Lee, S.B. Han, Y. Kim, J.T. Hong, M.K. Lee, B.Y. Hwang, Bioorg. Med. Chem. Lett. 26 (2016) 3351–3354.
[31] D.Q. Fei, L.L. Dong, F.M. Qi, G.X. Fan, H.H. Li, Z.Y. Li, Z.X. Zhang, Org. Lett. 18 (2016) 2844–2847.
[32] L.S. Wan, R. Chu, X.R. Peng, G.L. Zhu, M.Y. Yu, L. Li, L. Zhou, S.Y. Lu, J.R. Dong, Z.R. Zhang, Y. Li, M.H. Qiu, J. Nat. Prod. 79 (2016) 1628–1634.
[33] L.S. Wan, Y. Nian, X.R. Peng, L.D. Shao, X.N. Li, J. Yang, M. Zhou, M.H. Qiu, Org. Lett. 20 (2018) 3074–3078.
[34] Nanjing University of Chinese Medicine, Dictionary of Chinese Herb Medicines, second ed., Shanghai Scientific and Technologic Press, Shanghai, 2006, pp. 694–695.
[35] F. Liu, B. Dong, X. Yang, Y. Yang, J. Zhang, D.Q. Jin, Y. Ohizumi, D. Lee, J. Xu, Y. Guo, Bioorg. Chem. 77 (2018) 168–175.
[36] P. Wang, X. Yang, F. Liu, Y. Liang, G. Su, M. Tuerhong, D.Q. Jin, J. Xu, D. Lee, Y. Ohizumi, Y. Guo, Bioorg. Chem. 76 (2018) 53–60.
[37] B. Dong, L. An, X. Yang, X. Zhang, J. Zhang, M. Tuerhong, D.Q. Jin, Y. Ohizumi, D. Lee, J. Xu, Y. Guo, Bioorg. Chem. 87 (2019) 585–593.
[38] M.J. Frisch, G.W. Trucks, H.B. Schlegel, G.E. Scuseria, M.A. Robb, J.R. Cheeseman, G. Scalmani, V. Barone, B. Mennucci, G.A. Petersson, H. Nakatsuji, M. Caricato, X. Li, H.P. Hratchian, A.F. Izmaylov, J. Bloino, G. Zheng, J.L. Sonnenberg, M. Hada, M. Ehara, K. Toyota, R. Fukuda, J. Hasegawa, M. Ishida, T. Nakajima, Y. Honda, O. Kitao, H. Nakai, T. Vreven, J.A. Montgomery, Jr., J.E. Peralta, F. Ogliaro, M. Bearpark, J.J. Heyd, E. Brothers, K.N. Kudin, V.N. Staroverov, R. Kobayashi, J. Normand, K. Raghavachari, A. Rendell, J.C. Burant, S.S. Iyengar, J. Tomasi, M. Cossi, N. Rega, J.M. Millam, M. Klene, J.E. Knox, J.B. Cross, V. Bakken, C. Adamo, J. Jaramillo, R. Gomperts, R.E. Stratmann, O. Yazyev, A.J. Austin, R. Cammi, C. Pomelli, J.W. Ochterski, R.L. Martin, K. Morokuma, V.G. Zakrzewski, G.A. Voth, P. Salvador, J.J. Dannenberg, S. Dapprich, A.D. Daniels, O. Farkas, J.B. Foresman, J.V. Ortiz, J. Cioslowski, D.J. Fox, Gaussian 09, Revision A.02, Gaussian, Inc., Wallingford, CT, 2009.
[39] T. Bruhn, A. Schaumlöffel, Y. Hemberger, G. Bringmann, SpecDis, Version 1.62, University of Wuerzburg, Germany, 2014.
[40] J. Ma, Q. Ren, B. Dong, Z. Shi, J. Zhang, D.Q. Jin, J. Xu, Y. Ohizumi, D. Lee, Y. Guo, Bioorg. Chem. 76 (2017) 449–457.
[41] F. Liu, X. Yang, J. Ma, Y. Yang, C. Xie, M. Tuerhong, D.Q. Jin, J. Xu, D. Lee, Y. Ohizumi, Y. Guo, Bioorg. Chem. 75 (2017) 149–156.
[42] E.D. Garcin, A.S. Arvai, R.J. Rosenfeld, M.D. Kroeger, B.R. Crane, G. Andersson, G. Andrews, P.J. Hamley, P.R. Mallinder, D.J. Nicholls, S.A. St-Gallay, A.C. Tinker, N.P. Gensmantel, A. Mete, D.R. Cheshire, S. Connolly, D.J. Stuehr, A. Åberg, A.V. Wallace, J.A. Tainer, E.D. Getzoff, Nat. Chem. Biol. 4 (2008) 700–707.
[43] J. Xu, F. Ji, X. Sun, X. Cao, S. Li, Y. Ohizumi, Y. Guo, J. Nat. Prod. 78 (2015) 2648–2656.
[44] J. Ma, X. Yang, P. Wang, B. Dong, G. Su, M. Tuerhong, D.Q. Jin, J. Xu, D. Lee, Y. Ohizumi, J. Lin, Y. Guo, Bioorg. Chem. 75 (2017) 71–77.
[45] J.A. Marco, J.F. Sanz-Cervera, A. Yuste, Phytochemistry 45 (1997) 563–570.
[46] W.Y. Qi, W.Y. Zhang, Y. Shen, Y. Leng, K. Gao, J.M. Yue, J. Nat. Prod. 77 (2014) 1452–1458.
[47] X.L. Li, Y. Li, S.F. Wang, Y.L. Zhao, K.C. Liu, X.M. Wang, Y.P. Yang, J. Nat. Prod. 72 (2009) 1001–1005.
[48] V. Ravikanth, V.L. Niranjan Reddy, T. Prabhakar Rao, P.V. Diwan, S. Ramakrishna, Y. Venkateswarlu, Phytochemistry 59 (2002) 331–335.
[49] V. Ravikanth, V.L. Niranjan Reddy, A. Vijender Reddy, K. Ravinder, T. Prabhakar Rao, T. Siva Ram, K. Anand Kumar, D. Prakesh Vamanarao, Y. Venkateswarlu, Chem. Pharm. Bull. 51 (2003) 431–434.
[50] R. Upadhyay, E. Hecker, Phytochemistry 14 (1975) 2514–2515.
[51] A. Ahmed, M. Couladis, A. Mahmoud, A. De Adams, T. Mabry, Fitoterapia 70 (1999) 140–143.
[52] K. Toume, T. Nakazawa, T. Hoque, T. Ohtsuki, M.A. Arai, T. Koyano, T. Kowithayakorn, M. Ishibashi, Planta Med. 78 (2012) 1370–1377.
[53] M.B. Gewali, M. Hattori, Y. Tezuka, T. Kikuchi, T. Namba, Chem. Pharm. Bull. 37 (1989) 1547–1549.
[54] M. Tada, H. Seki, Agric. Biol. Chem. 53 (1989) 425–430.
[55] A.R. Lal, R.C. Cambie, P.S. Rutledge, P.D. Woodgate, C.E.F. Rickard, G.R. Clark, Tetrahedron Lett. 30 (1989) 3205–3208.
[56] F. He, J.X. Pu, S.X. Huang, W.L. Xiao, L.B. Yang, X.N. Li, Y. Zhao, J. Ding, C.H. Xu, H.D. Sun, Helv. Chim. Acta 91 (2008) 2139–2147.
[57] J.X. Zhao, C.P. Liu, W.Y. Qi, M.L. Han, Y.S. Han, M.A. Wainberg, J.M. Yue, J. Nat. Prod. 77 (2014) 2224–2233.
[58] Z.Q. Lu, G.T. Chen, J.Q. Zhang, H.L. Huang, S.H. Guan, D.A. Guo, Helv. Chim. Acta 90 (2007) 2245–2250.
[59] W.S. Suh, K.J. Park, D.H. Kim, L. Subedi, S.Y. Kim, S.U. Choi, K.R. Lee, Bioorg. Chem. 72 (2017) 156–160.
[60] S.R. Lee, S. Lee, E. Moon, H.J. Park, H.B. Park, K.H. Kim, Bioorg. Chem. 70 (2017) 94–99.
[61] A.T. Kim, D.O. Kim, Int. J. Biol. Macromol. 133 (2019) 732–738.
[62] H.A. Stefani, K. Gueogjan, F. Manarin, S.H. Farsky, J. Zukerman-Schpector, I. Caracelli, S.R. Pizano Rodrigues, M.N. Muscará , S.A. Teixeira, J.R. Santin, I.D. Machado, S.M. Bolonheis, R. Curi, M.A. Vinolo. Eur. J. Med. Chem. 58 (2012) 117–127.